Key Resources Table

Reagent type or resource	Designation	Source or reference	Identifiers & Additional information
Vector	pDONR-Zeo	Thermo Fisher	
Vector	Ubq-GFPCT Gateway vector	(Basto et al., 2008)	
Vector	Ubq-mCherryCT Gateway vector	(Basto et al., 2008)	
Vector	pRNA-mKate2CT Gateway vector	(Novak et al., 2016)	
cDNA	*spd-2* (pOT2 vector)	Geneservice Ltd	Clone LD24702
Primer	Spd-2_AttB_FP_mutant	This study	GGGGACAAGTTTGTACAAAA AAGCAGGCTTCACAAGTTTGT ACAAAAAAGCAGGCTTCATG GACACTACCAGTGGAAGCC
Primer	Spd-2_AttB_FP_WT	This study	GGGGACAAGTTTGTACAAAA AAGCAGGCTTCACAAGTTTGT ACAAAAAAGCAGGCTTCATG GACAGTAGCAGTGGAAGCC
Primer	Spd-2_AttB_RV	This study	GGGGACCACTTTGTACAAGA AAGCTGGGTCAAATTTAAAAC TAATCGGGACACTGATGC
Primer	M1F spd-2 S121A	This study	CCAAGGGCACAAACATCGCT TTTGAGCCTGCGGAG
Primer	M1R rev spd-2 S121A	This study	CTCCGCAGGCTCAAAAGCGA TGTTTGTGCCCTTGG
Primer	M2F spd-2 T329A	This study	CCAGAAAGTAACGTGGCTCT GGATTCGGTTGGCGAG
Primer	M2R rev spd-2 T329A	This study	CTCGCCAACCGAATCCAGAG CCACGTTACTTTCTGG
Primer	M3F spd-2 S397A	This study	CGAGATCCTAAGTCTCGCCG CGATCGACAAGGCGC
Primer	M3R rev spd-2 S397A	This study	GCGCCTTGTCGATCGCGGCG AGACTTAGGATCTCG
Primer	M4F spd-2 S484A	This study	CGCGCAAGCCGCTCGCTCCG CTGGCGGACCATC
Primer	M4R rev spd-2 S484A	This study	GATGGTCCGCCAGCGGAGC GAGCGGCTTGCGCG
Primer	M5F spd-2 S569A	This study	GCCAGTGAACAAGAAGAGGG TTGCGATCGCTACAATGGG
Primer	M5R rev spd-2 S569A	This study	CCCATTGTAGCGATCGCAAC CCTCTTCTTGTTCACTGGC

Primer	M6F spd-2 S614A, S617, S618A	This study	CTGGCCAAAAATCTAGCGCCCCTGGCCGCGCCAAGAAGCTGTCTC
Primer	M6R rev spd-2 S614A, S617, S618A	This study	GAGACAGCTTCTTGGCGCGGCCAGGGGCGCTAGATTTTTGGCCAG
Primer	M7F spd-2 T672A, S673A and S674A	This study	GGAAGACGTGGGTTGGGAGCCGCCGCTGTTGCAGTGCCACGTAG
Primer	M7R rev spd-2 T672A, S673A and S674A	This study	CTACGTGGCACTGCAACAGCGGCGGCTCCCAACCCACGTCTTCC
Primer	Spd2S625A_FW	This study	CCTGTCCTCGCCAAGAAGCTGTCTCTCGGCGCCGCTGCTGGACAGCACAACCAGTTCC
Primer	Spd2S625A_RV	This study	GGAACTGGTTGTGCTGTCCAGCAGCGGCGCCGAGAGACAGCTTCTTGGCGAGGACAGG
Primer	Spd2T516A_FW	This study	CAGAAGCCGAGGCGGACATCGATGAGTGGCCCTCGGCGCCGGTAAAGGAGCCTAGCCGCAGAGTGAGACG
Primer	Spd2T516A_RV	This study	CGTCTCACTCTGCGGCTAGGCTCCTTTACCGGCGCCGAGGGCCACTCATCGATGTCCGCC
Primer	pRNA_PCR_FW	This study	GACCCAGCTTTCTTGTACAAAGTG
Primer	pRNA_PCR_RV	This study	GAAGCCTGCTTTTTTGTACAAACTTG
Primer	Spd2_Insert1m_FW	This study	TGTACAAAAAAGCAGGCTTCATGGACACTACCAGTGGAAG
Primer	Spd2_Insert1146_RV	This study	TGTACAAGAAAGCTGGGTCAAATTTAAAACTAATCGGGACACTGATGC
Primer	Spd2_Insert1wt_FW	This study	TGTACAAAAAAGCAGGCTTCATGGACAGTAGCAGTGGAAG
Primer	Spd2_Insert552_FW	This study	CTGCACCGAGGATGAAAACGATGAGGAGGA
Primer	Spd2_Insert552_RV	This study	TCCTCCTCATCGTTTTCATCCTCGGTGCAG
Fly line	Ubq-Spd-2-GFP	(Dix and Raff, 2007)	Spd-2-WT-GFP
Fly line	Ubq-Spd-2^{11A}-GFP	This study	Spd-2-11A-GFP
Fly line	Ubq-Spd-2^{CONS}-GFP	This study	Spd-2-CONS-GFP
Fly line	Ubq-Spd-2^{ALL}-GFP	This study	Spd-2-ALL-GFP
Fly line	Ubq-Spd-2-mCherry	This study	Spd-2-WT-mCherry

Fly line	Ubq-Spd-2^{CONS}-mCherry	This study	Spd-2-CONS-mCherry
Fly line	Ubq-Spd-2^{ALL}-mCherry	This study	Spd-2-ALL-mCherry
Fly line	Ubq-Jupiter-mCherry	(Callan et al., 2010)	
Fly line	ePolo-GFP(Trap)	(Buszczak et al., 2006)	
Fly line	Ubq-RFP-Cnn	(Conduit and Raff, 2010)	
Fly line	Aur-A-GFP	(Lucas and Raff, 2007)	
Fly line	*spd-2^{z35711}*	(Giansanti et al., 2008)	
Fly line	*spd-2^{G20143}*	(Dix and Raff, 2007)	
Fly line	*spd-2$^{Df(3L)st-j7}$*	Bloomington Stock Center	Stock #5416
Fly line	*cnn^{f04547}*	(Lucas and Raff, 2007)	
Antibody	Rabbit anti-Spd-2	(Dix and Raff, 2007)	Animal#SK3428; Lab ID: Ab#57; 1:500
Antibody	Rabbit anti-Cnn	(Lucas and Raff, 2007)	Animal#SK3516; Lab ID: Ab#37, 1:1000
Antibody	Mouse anti-γ-tubulin	Sigma	GTU-88; T6557; 1:500
Antibody	Mouse anti-Actin	Sigma	A3853; 1:2000
Antibody	Rabbit anti-GAGA factor	(Raff et al., 1994)	Z13-3; Lab ID: Ab#144; 1:500
Antibody	Mouse anti-α-tubulin	Sigma	DM1a; T9026-.2ML; 1:500
Antibody	Guinea pig anti-Cnn	(Lucas and Raff, 2007)	Animal#SK42; Lab ID: Ab#55; 1:1000
Antibody	Rabbit anti-Cnn pSer567	(Feng et al., 2017)	Animal#30129; Lab ID: Ab#236; 1:500
Antibody	Sheep ECL anti-Mouse HRP-conjugated	GE Healthcare Life Sciences, Sigma	NA931V
Antibody	Donkey ECL anti-Rabbit HRP-conjugated	GE Healthcare Life Sciences, Sigma	NA934V
Antibody	Swine anti-Rabbit HRP conjugated	Dako, Agilent Technologies	P0399; 1:3000
Antibody	Goat anti-Mouse IgG Alexa Flour 594	Invitrogen, Thermo Fisher	A11032; 1:500
Antibody	Llama GFP-Booster Atto488	Chromotek	gba488; 1:500

Antibody	Goat anti-Rabbit IgG Alexa Flour 594	Invitrogen, Thermo Fisher	A11012; 1:500
Antibody	Donkey anti-Guinea Pig IgG(H+L) CF405S	Biotium	20356; 1:500
Mounting medium	Vectashield without DAPI	Vector Laboratories	H-1000
Mounting medium	Vectashield with DAPI	Vector Laboratories	H-1200
Chemicals	Alkaline phosphatase	Roche Diagnostics	10713023 001
Chemicals	Phosphatase inhibitor cocktais 2 and 3	Sigma	P5726-1ML, P0044-1ML
Chemicals	Protein A Dynabeads (Life Technologies)	Thermo Fisher	10002D
Chemicals	BS3 crosslinker	Thermo Fisher	21580
Commercial assay or kit	SuperSignal West Femto kit	Thermo Fisher	34095
Commercial assay or kit	NEBuilder® HiFi DNA Assembly Master Mix	New England Biolabs	E2621S
Commercial assay or kit	Gateway BP Clonase Enzyme mix	Thermo Fisher	11789100
Commercial assay or kit	Gateway LR Clonase Enzyme mix	Thermo Fisher	11791100
Commercial assay or kit	QuikChange Multi Site-Directed Mutagenesis kit	Agilent Technologies	200515
Commercial assay or kit	QuikChange II XL Site-Directed Mutagenesis kit	Agilent Technologies	200521
Commercial assay or kit	mMESSAGE mMACHINE T3 kit	Thermo Fisher	AM1348
Centrifuge	Beckman SW 41 Ti Rotor	Beckman Coulter	
MS/MS	LTQ Orbitrap Mass Spectrometer, UltiMate 3000 Nano LC system	Thermo Scientific, Advanced Proteomics Facility Oford	
Microscope	Perkin Elmer ERS Spinning Disk confocal system	PerkinElmer Inc.	
Microscope	Zeiss Axioskop 2 microscope	Zeiss International	
Microscope	DeltaVision OMX V3 Blaze microscope	GE Healthcare Life Sciences; Micron Oxford	29065721
Microscope	Zeiss 880 Airyscan microscope	Zeiss International; Micron Oxford	

Software	Jalview	(Waterhouse et al., 2009)	Version 2.10.4b1
Software	Mascot software	Matrix Science	
Software	ImageJ	NIH	Version 2.0.0
Software	Volocity	PerkinElmer Inc.	Version 6.3
Software	softWoRx	GE Healthcare Life Sciences	Version 6.1
Software	SIM-Check	(Ball et al., 2015)	
Software	OMX Editor	Micron Oxford	https://github.com/MicronOxford/OMXeditor
Software	Chromagnon	(Matsuda et al., 2018)	https://github.com/macronucleus/Chromagnon
Software	ZEN	Zeiss International	Black edition
Software	Prism 7	GraphPad	Version 7
Software	R	R Core Team (2013)	http://www.R-project.org/
Software	OMERO	(Allan et al., 2012)	Version 5.4.5
Software	Illustrator/Photoshop	Adobe	CS6

Fly husbandry, stocks and handling

Flies were kept at 25°C or 18°C on *Drosophila* culture medium (0.77% agar, 6.9% maize, 0.8% soya, 1.4% yeast, 6.9% malt, 1.9% molasses, 0.5% propionic acid, 0.03% ortho-phosphoric acid and 0.3% nipagin). Stocks were kept in 8 cm x 2.5 cm plastic vials or 0.25-pint plastic bottles. Embryos were collected on cranberry-raspberry juice plates (25% cranberry-raspberry juice, 2% sucrose and 1.8% agar) supplemented with fresh yeast. Standard fly handling techniques were employed (Roberts, 1998). *In vivo* studies were performed using 1.5-2 h-old syncytial blastoderm stage embryos. After 0-1 h collections at 25°C, embryos were aged at 25°C for 45-60 min. When injecting mRNA, embryos were collected for 20 min, injected, and imaged after 120-150 min at 21°C (but always within the syncytial blastoderm stage of development). Prior to injection or imaging, embryos were dechorionated by using double-sided tape onto a slide and mounted on a strip of glue onto a 35 mm glass bottom petri dish with a 14 mm micro-well (MatTek). After desiccation for 1 min (non-injection experiments) or 3 min (pre-mRNA injection) at 25°C, embryos were covered in Voltalef oil (ARKEMA). Live imaging was performed using either the spinning disk confocal or the 3D-SIM systems described below.

Transgenic *Drosophila* lines

Potential Polo binding sites in the amino acid sequence of *Drosophila melanogaster* Spd-2 were identified by searching for the consensus Polo binding motif S-S/T. Site conservation was assessed using FlyBase BLAST (selecting the genus *Drosophila*) and Jalview for protein alignment. The ALL and CONS constructs were designed *in silico*

and synthesised externally by GENEWIZ Co. Ltd. (Suzhou, China); the WT *spd-2* cDNA was obtained from Geneservice Ltd (UK). The WT, ALL and CONS Spd-2 cDNAs were cloned into a pDONR-Zeo vector and then introduced in Ubq-GFPCT and Ubq-mCherryCT destination vectors via Gateway cloning as indicated (Key Resources Table). The Ubq-Spd-2-11A-GFP plasmid was derived via site-directed mutagenesis on pDONRSpd-2 vector using QuikChange Multi Site-Directed mutagenesis followed by Gateway cloning into the Ubq-GFPCT vector. The plasmids were sent to BestGene Inc. (Chino Hills, California) or the University of Cambridge Genetics Fly Facility (UK) for generation of the transgenic lines via random P-element insertion in to a w1118 background. Other GFP, RFP, and mCherry lines have been described previously (see Key Resources Table). For the *Spd-2* mutant embryo analyses we used embryos laid by *spd-2*^{Z35711}/*spd-2* $^{Df(3L)st-j7}$ or *spd-2*^{Z35711}/*spd-2*^{G20143} transheterozygotes expressing two copies of the Spd-2-GFP fusions, or one copy of a Spd-2 fusion and one copy of another fusion protein. *Drosophila melanogaster Oregon-R* and *w*^{67} were used as a WT stock where indicated. Balancer chromosomes and markers used were described previously (FlyBase, USA).

Centrosome Purification

Whole centrosomes were isolated from extracts of early *Drosophila* embryos (0-4 h) using a modified version of a centrosome isolation protocol (Lehmann et al., 2006). Embryo extract containing 50% sucrose was layered on top of a sucrose cushion comprising 55% and 70% sucrose. The tubes were spun at 27,000 rpm, causing the centrosomes in the extract to move through the 55% layer and into the 70% sucrose

layer. A “Cytosolic” fraction was collected from the top of the tube, and fractions were then collected from the bottom of the tube. Western blotting was performed to identify the “Centrosome” fractions that contained the greatest enrichment of centrosomal proteins. Phosphatase treatment was carried out on the centrosome fractions using alkaline phosphatase (Roche) for 4.5 hr at 37°C with or without phosphatase inhibitor cocktails 2 and 3 (Sigma).

Centrosome immunoprecipitation and Mass Spectrometry

Centrosomes were immunoprecipitated from the centrosomal fractions using anti-Cnn antibodies coupled to protein A conjugated magnetic Dynabeads (Life Technologies). Cytoplasmic Spd-2 was immunoprecipitated from the cytoplasmic fractions using anti-Spd-2 antibodies coupled to Dynabeads. The dynabead/antibody suspensions were rotated at 4°C overnight. The antibodies were cross-linked to the beads using the BS3 crosslinker (Thermo Fisher). Centrosomal and cytoplasmic fractions were diluted 1:1, added to the antibody-crosslinked beads and rotated at 4°C for 2 h. Beads were washed, boiled in sample buffer (SB) and separated on a polyacrylamide gel, and the band containing Spd-2 was cut out. Samples were prepared for mass spectrometry and enriched for phosphopeptides as described previously (Conduit et al., 2014a). Liquid chromatography-MS/MS analysis was performed using a LTQ Orbitrap Mass Spectrometer (Thermo Scientific) coupled to an UltiMate 3000 Nano LC system (Thermo Scientific). The mass spectrometry data were searched against the FlyBase sequence database (http://flybase.bio.indiana.edu/) using Mascot software (Matrix Science). The following settings were used for the searches: enzyme: trypsin;

fixed modification: carbamidomethylation; variable modifications: methionine oxidation, glutamine/asparagine deamidation; serine/threonine/tyrosine phosphorylation; error tolerance for the precursor ions, 20 ppm; mass error tolerance for the fragment ions, 0.6 Da; number of missed cleavage sites, 3. The MS/MS spectra for identified phosphopeptides were manually inspected in Mascot.

Western blot analysis

Western blotting to estimate embryonic protein levels was performed as described previously (Novak et al., 2014). The following primary antibodies were used for western blot analysis (see Key Resources Table): rabbit anti-Spd-2 (1:500), rabbit anti-Cnn (1:1000), mouse anti-γ-tubulin (1:500), mouse anti-Actin (1:2000), and rabbit anti-GAGA factor (1:500). HRP conjugated secondary antibodies used (all at 1:3000): swine anti-rabbit (Dako), or ECL anti-mouse and ECL anti-rabbit (GE Healthcare).

RNA synthesis and microinjection

The mRNA injection assay and the modified pRNA destination vector with the C-terminal mKate2 tag used here have been described previously (Novak et al., 2014; 2016). Spd-2-ALL and Spd-2-CONS cDNA were introduced into the vector via Gateway cloning. 2 point mutations were introduced into WT Spd-2-mKate2 using QuikChange mutagenesis (Agilent) to generate Spd-2-AA-mKate2. Spd-2-N-term-mKate2 and Spd-2-C-term-mKate2 partial mutants were derived from PCR-amplified fragments of WT Spd-2-mKate2 and Spd-2-ALL-mKate2 via NEBuilder HiFi assembly (New England Biolabs). The last potential binding site mutated in the N-terminus group was S538-

S540, and the first potential binding site mutated in the C-terminus group was S581-S582, so that each group would include 17 potential sites. *In vitro* RNA synthesis was performed using a T3 mMESSAGE mMACHINE kit (Thermo Fisher) and RNA was purified using an RNeasy MinElute kit (Qiagen). All RNA constructs were injected at a concentration of 2 mg/ml.

Immunofluorescence

Embryos were collected for 0-1 h, aged for 45-60 min, and processed as described (Stevens et al., 2010). Samples were mounted onto microscopy slides with high-precision glass coverslips (CellPath). Specifics for each experiment as follows:

Quantification of successful completion of pronuclear fusion

Embryos were stained using a mouse anti-α-tubulin (1:1000), followed by Alexa 594nm anti-mouse and GFP-Booster Atto488 (1:500 dilution). Samples were mounted in Vectashield medium with DAPI. Embryos were counted using a Zeiss Axioskop 2 microscope (Zeiss International) with a 10x/0.30-NA and a 40x/0.75-NA objectives. Embryos were counted as developing beyond pronuclear fusion if they had clearly reached syncytial/gastrulation stages. For each of the 4 conditions (non-rescue, WT-rescue, CONS-rescue and ALL-rescue) we preformed 2 biological replicates (embryos from separate sets of mothers), each with 3 technical replicates (embryos collected and processed independently); >50 embryos were counted per sample.

Phospho-Cnn staining

Embryos were stained using a guinea pig anti-Cnn antibody (1:1000) and a rabbit anti-Cnn pSer567 antibody (1:500); followed by Alexa 594nm anti-rabbit, CF405S anti-guinea pig, and GFP-Booster Atto488 (1:500 dilution). Samples were mounted in Vectashield medium without DAPI.

γ-tubulin staining

Embryos were stained using a mouse anti-γ-tubulin antibody (1:500), followed by Alexa 594nm anti-mouse and GFP-Booster Atto488 (1:500 dilution). Samples were mounted in Vectashield medium with DAPI.

Imaging

Spinning disk confocal microscopy

Embryos were imaged at 21°C on a Perkin Elmer ERS spinning disk (Volocity software) mounted on a Zeiss Axiovert 200M microscope using a 63X/1.4-NA oil immersion objective and an Orca ER CCD camera (Hamamatsu Photonics, Japan). 488- and 568-nm lasers were used to excite GFP and RFP/mCherry, respectively. Confocal sections of 13 slices with 0.5-µm-thick intervals were collected every 30 s (17 slices for the analysis of protein dynamics throughout the cell cycle). Focus was occasionally manually readjusted in between intervals.

3D-SIM

3D-SIM microscopy was performed and analysed as described (Conduit et al., 2014a) on an OMX V3 Blaze microscope (GE Healthcare, UK) with a 60x/1.42-NA oil

UPlanSApo objective (Olympus); 405-, 488- and 593-nm diode lasers, and Edge 5.5 sCMOS cameras (PCO). The raw acquisition was reconstructed using softWoRx 6.1 (GE Healthcare) with a Wiener filter setting of 0.006 and channel- specific optical transfer function. Living embryos were imaged at 21°C, acquiring stacks of 6 z-slices (0.125-µm intervals). Stacks of 13 z-slices (0.125-µm intervals) were acquired from fixed samples (phospho-Cnn staining, the images shown are maximum intensity projections). For multi-colour 3D-SIM, images from the different colour channels were registered with alignment parameters obtained from calibration measurements using 1µm to 0.2µm TetraSpeck Microspheres (Thermo Fisher) using OMX Editor and Chromagnon alignment software. The SIM-Check plug-in in ImageJ (NIH) was used to assess the quality of the SIM reconstructions (Ball et al., 2015).

Airyscan

Fixed samples (γ-tubulin staining) were imaged using an inverted Zeiss 880 microscope fitted with an Airyscan detector. The system was equipped with Plan-Apochromat 63x/1.4-NA oil lens. The laser excitation lines used were 405nm diode, 488nm argon and 561nm diode laser. Stacks of 25 slices with 0.14-µm-thick intervals were collected with pixel size (xy) of 0.035 µm, using a piezo-driven z-positioner stage. Images were Airy-processed in 3D with a strength value of “auto” (~6). The software used to acquire images and process the images taken in super-resolution Airyscan mode was ZEN (black edition, Zeiss).

Image and statistical analysis

Blind analysis of 3D-SIM images

Centrosome images were selected based on quality of the reconstruction as assessed by the SIM-Check plug-in and the presence of a visible, well-formed ring corresponding to the presence of protein at the mother centriole wall. Each individual centrosome image was saved as a separate file, renamed and randomised post acquisition. The entire dataset for each experiment was scored blindly. The Spd-2-GFP datasets (mutant or WT backgrounds) were scored once. They each included 3 different conditions (WT, CONS and ALL) with 36 centrosomes per condition. The Spd-2-mCherry/Polo-GFP dataset included 2 conditions (WT and CONS), with 30 images per condition (15 individual centrosomes, 2 different channels); it was scored independently by 3 different people, and an average score was calculated.

Analysis of centrosome and MT fluorescent intensities

We used ImageJ to calculate the maximum intensity projection of z-stacks of movies taken from the PE spinning disk system. The time frame chosen for analysis corresponded to 1 min before nuclear envelope breakdown. The 5 brightest centrosomes per embryo were identified via manual thresholding and analysed; the number of embryos analysed is indicated in each Figure. For both the green and red channels we measured the mean intensity within a square of fixed size (5.04 μm x 5.04 μm) centred manually on each individual centrosome. Similarly, we measured the mean intensity of the background near each centrosome. We calculated the average centrosome intensity and subtracted the average background intensity per embryo. The values for all the embryos were plotted on Prism 7 (GraphPad Software). Prism was

also used to check column statistics and Gaussian distribution of the data. For the Jupiter-mCherry/Spd-2-GFP data we used the D'Agostino–Pearson omnibus normality test. For the statistical analysis, we used ordinary One-Way ANOVA with Tukey's multiple comparisons test if data passed the normality test, or the Kruskal-Wallis test with Dunn's multiple comparisons test otherwise. For the dataset comparing Spd-2-GFP and Spd-2-11A-GFP we used the Shapiro-Wilk normality test followed by the unpaired t test with Welch's correction. Significance in statistical tests was defined by $P < 0.05$.

Radial profiling of centrosomes

We used ImageJ to calculate an average "radial profile" of the distribution of the different PCM proteins around the mother centriole (Conduit et al., 2014b). For embryos imaged live, the 5 brightest centrosomes in each embryo were analysed (the number of embryos analysed for each genotype is indicated in the individual Figures). For the analysis of fixed embryos, we analysed 1 pair of centrosomes per embryo, 5 embryos per technical replicate (embryos collected and processed independently), and 3 technical replicates in total per condition (so total centrosomes analysed = 15).

For each individual centrosome we found its center of mass by thresholding the image and running the ''analyse particles'' (centre of mass) macro on the most central Z plane of the centrosome, as described (Conduit et al., 2014b). We then centred concentric rings spaced at 0.021 μm and spanning across 2.09 μm on this centre (0.007 μm and spanning across 1.41 μm for the fixed γ-tubulin images) and measured the average fluorescence in each ring, and subtracted the average cytosolic signal. Each individual

centrosome profile was then normalised to the average peak intensity for all the centrosomes of the control condition (WT Spd-2-GFP embryos). Each profile was then mirrored to produce a full centrosome profile. The final radial profiles shown are an average of all the full centrosomal profiles per condition. In some graphs we show a "normalised" profile, where each individual centrosome profile was normalised to the average peak intensity of its corresponding condition (rather than to the WT Spd-2-GFP embryo control). The resulting radial profile peaks for all conditions were then normalised to 1; this allows the distribution of different proteins around the centriole to be compared, independently of differences in centrosomal protein levels.

Analysis and regression modelling for the dynamics of Spd-2-GFP

Spd-2-GFP dynamics throughout the cell cycle were analysed as described (Aydogan et al., 2018). Briefly, we used ImageJ to calculate the maximum intensity projection of z-stacks of movies taken from the PE spinning disk system. The backgrounds were subtracted using the subtract background function with a rolling ball radius of 10 pixels. Spd-2-GFP foci (centrosomes) were tracked using TrackMate plug-in (Tinevez et al., 2016) with the following analysis settings: track spot diameter size of 2.1 μm, initial threshold of 0, and quality of >0.03. Regression analysis on the centrosome growth curves were carried out using Prism, and the mathematical modelling was done using the nonlinear regression (curve fit) analysis function, excluding the last 3 points (90s) of the cell cycle (as the data was very variable towards the end of mitosis).

The data for WT Spd-2-GFP (Figure 8, *blue line*) was fitted against four different functions to assess the most suitable model (Figure S7A): (1) linear growth followed by linear decrease; (2) linear growth followed by plateau followed by linear decrease; (3) Gaussian function; (4) Lorentzian function. Functions (1) and (2) are bespoke algorithms, with the following equations for *X* amount of time:

(1)

$$Y_1 = intercept_1 + slope_1 * X$$

$$Y_{X0} = slope_1 * X_0 + intercept_1$$

$$Y_2 = Y_{x0} + slope_2 * (X - X_0)$$

$$Y = IF(X < X_0, Y_1, Y_2)$$

(2)

$$Y_1 = intercept_1 + slope_1 * X$$

$$Y_{X0} = slope_1 * X_0 + intercept_1$$

$$Y_2 = Y_{X0} + slope_2 * (X - X_0)$$

$$slope_2 = 0$$

$$Y_{X1} = Y_{X0} + slope_2 * (X_1 - X_0)$$

$$Y_3 = Y_{X1} + slope_3 * (X - X_1)$$

$$Y = IF(X < X_0, Y_1, IF\ (X < X_1, Y_2, Y_3))$$

The only constraints applied to these equations were the requirements for the slopes and inflection points (X_0, X_1) to be greater than 0. Centrosomes that come from a single embryo were treated as internal replicates, and thus the fitting used only the mean *Y* value of each time point. To judge and control the quality and precision of regression

(goodness-of-fit), we used the R^2, adjusted R^2, and absolute sum-of- square values. To compare the fits, the extra sum-of-squares F test was applied, and the appropriate fit was chosen by selecting the simpler model unless $P < 0.05$. The “linear growth followed by plateau followed by linear decrease” model best fit the data (Figure S7A), but it is likely a simplification of a more complex model, so individual curves are shown for each embryo without any model fitted (average of >44 centrosomes per embryo) (Figure S3).

The data for Spd-2-CONS-GFP (Figure 8, *red line*) was fitted against the “linear growth followed by plateau followed by linear decrease” model, as this was the preferred model for the WT data. As this data seemed to better be described as a straight line, this model was also compared to a standard straight line model (with no slope constraints)—function (5); or a user-defined constant line function (6) (Figure S7B):

(6)

$$Y = intercept_1 + 0 * X$$

The preferred model was the straight line—function (5) (Figure S7B)—although the average slope value was nearly zero (-0.0005 $\pm$ 0.0054; mean $\pm$ SD), indicating that the appropriate model in practice would be a constant line.

Supplementary Tables

Table S1: *Spd-2 sites phosphorylated at the centrosome*			
Peptide sequence	**Peptide score**	**High-scoring phosphorylated site**	**Additional sites mutated**
GTNI**S**FEPAEITGR	53.03	S121	-
TNQPLLEPESNV**T**LDSVGEK	65.26	T329	-
RPPSSSEILSL**S**AIDK	38.85	S397	-
KPL**S**PLADHPQITISR	34.55	S484	-
RV**S**IATMGLIPR	29.93	S569	-
NL**S**PL**S**SPR	42.33	S614	S617, S618
GLG**T**S**S**VAVPR	64.8	S673	T671, S672

Table S1

Identification of Spd-2 sites phosphorylated at the centrosome. The Table lists amino acids in Spd-2 that were identified as being phosphorylated in the centrosomal fractions of embryo extracts, but not the cytosolic fractions, by Mass Spectroscopy. The Peptide score is the Mascot Ion Score (Koenig et al., 2008)—scores >29 indicate identity or extensive homology ($p<0.05$). Phosphorylated amino acids are marked in *red*. These sites were mutated together with an additional 4 Ser/Thr resides that could potentially have been phosphorylated in these peptides (*blue*) to generate Spd-2-11A-GFP.

Table S2: *Potential Polo binding sites in Spd-2 previously reported to be phosphorylated*				
Peptide sequence	**Phospho sites**	**Other phospho sites**	**Ref.**	**Also**
VFGDL**SS**F**S**KGRR	S34 S35	(S37)	(Zhai et al., 2008)	-
ALETLEKPRP**S**RS**S**QAK	S76	S73	(Bodenmiller et al., 2007)	-
EKP**S**L**S**VAEILKS**S**FVEK	(S156)	S146 S148	(Zhai et al., 2008)	(Bodenmiller et al., 2007)
SENIWNIV**S**N**SS**PNR**S**R	(S310) (S311)	(S308) S315		(Bodenmiller et al., 2007)
RPP**SSS**EIL**S**L**S**AIDK	(S389) (S390) (S391)	(S395) S397		(Bodenmiller et al., 2007)
DIDLN**S**D**T**S**T**VEVVNHLWEHGR	(S413) (T414)	S410 (T412)		-
AD**T**DPVE**T**EAEADIDEWP**ST**PVK EP**S**RR	(S515) (T516)	T499 T504 S522		-
AA**S**P**SSS**DGVRPL**T**C**T**EDENDEE DEDK**T**PVNKK	S538 S539 (S540)	S536 (T547) (T549) T561		-
KA**SS**L**S**STRLDGCDVAVASSTER	S581 S582	(S584)		-
NL**S**PL**SS**PR	S617 S618	S614		(Bodenmiller et al., 2007)
SCL**SS**PLLD**ST**TSSDRR	S624 S625 (S630) (T631)			-
KANSSPAG**S**EAS**S**TSGFTASGR	(S658)	S654		-
RGLG**T**S**S**VAVPR	(S673) S674	(T672)		This study, (Habermann et al., 2012)
SCLSSPLLDSTTS**S**DRR	S634		(Habermann et al., 2012)	-

Table S2

Several potential PBD binding sites have previously been identified in Spd-2. The Table lists several previously identified Spd-2 peptides that include the potential PBD binding motif S-S/T(p). Definitively identified phosphorylated sites within PBD binding motifs are shown in red; in cases where there is some ambiguity about the phosphorylated sites the amino acids are shown in *blue*, and these sites are listed in brackets. Other phosphorylated sites which are on the same reported peptide, but are not part of a PBD binding motif, are shown in bold. The phospho-proteomic screens in which these peptides were identified are listed.

Supplementary Figure Legends

Figure S1

Mutation of several centrosomal phosphosites in Spd-2 appears to have only a small effect on the centrosomal function of Spd-2 *in vivo*. **(A)** Western blot analysis of WT or *Spd-2* mutant larval brain cells expressing either Spd-2-GFP or Spd-2-11A-GFP (as indicated). **(B)** Micrographs show stills of living *Spd-2* mutant embryos expressing either Spd-2-GFP or Spd-2-11A-GFP, imaged on a spinning disk confocal microscope. Both constructs efficiently rescue the *Spd2* mutant embryos (data not shown), which normally do not develop due to a failure in pronuclear fusion (Dix and Raff, 2007). **(C)** Micrographs show a magnified view of centrosomes, highlighting that although WT Spd-2-GFP and Spd-2-11A-GFP are both highly concentrated at centrosomes, a small number of "flares" of Spd-2-11A-GFP can be detected that are constantly being ejected from the centrosomes (arrowheads); such Spd-2 flaring can occur when the PCM matrix has been weakened (Conduit et al., 2014b) **(D)** Graph quantifies the centrosomal fluorescent intensity of either Spd-2-GFP or Spd-2-11A-GFP at mid-late S-phase in *Spd-2* mutant embryos (in arbitrary fluorescence units [a.u.], WT normalised to 1. Data was collected from 5 embryos (10 centrosomes per embryo were analysed), bars represent mean ± SEM. The Shapiro-Wilk normality test was used to check Gaussian distribution of the data. The difference between the two datasets was determined to be statistically significant using the unpaired t test with Welch's correction (*, $P<0.05$).

Figure S2

Abnormal Polo-GFP and Spd-2-mCherry distribution and mitotic defects in *Spd-2* mutant embryos rescued with Spd-2-CONS-mCherry or Spd-2-ALL-mCherry.

Micrographs show stills of living Spd-2 mutant embryos expressing Polo-GFP (*green*) and either WT Spd-2-mCherry, Spd-2-CONS-mCherry or Spd-2-ALL-mCherry (*red*, as indicated). Images are maximum intensity projections of z-stacks acquired on a spinning disk confocal microscope. Most embryos rescued with Spd-2-ALL-mCherry did not develop to syncytial blastoderm stages and the few that did exhibited severe defects (as in the example shown here), making it difficult to accurately stage the embryos.

Figure S3

Centrosome maturation in Spd-2 mutant embryos rescued by WT Spd-2-GFP. Graphs show the mean centrosomal Spd-2-GFP intensity (in arbitrary units [a.u.]) through an entire embryonic cell cycle for 14 different WT Spd-2-GFP embryos. Bars indicate SD (number of centrosomes analysed per embryo=52-171). Time (s) is indicated; t=0 was set as the time that centrosomes first separated at the start of S-phase. Dashed lines indicate nuclear envelope breakdown (NEB).

Figure S4

Centrosome maturation in Spd-2 mutant embryos rescued by Spd-2-GFP-CONS. Graphs show the mean centrosomal Spd-2-GFP-CONS intensity (in arbitrary units [a.u.]) through an entire embryonic cell cycle for 14 different Spd-2-GFP-CONS embryos. Bars indicate SD (number of centrosomes analysed per embryo=44-124).

Time (s) is indicated; t=0 was set as the time that centrosomes first separated at the start of S-phase. Dashed lines indicate nuclear envelope breakdown (NEB).

Figure S5

An alignment of the known PBD binding motifs from human Cep192 and *C. elegans* SPD-2 with *Drosophila* Spd-2. A multiple sequence alignment (MSA) of the amino acid sequence of the two isoforms of human Cep192, *C. elegans* SPD-2 and 13 different Spd-2 homologues from various *Drosophila* species. The previously identified Polo-binding sites in human Cep192 and *C. elegans* SPD-2 are indicated in boxes (*red* and *blue*, respectively), and the potential corresponding *Drosophila* sequences, if any, are highlighted in the larger surrounding boxes. Note that no clear *Drosophila* motifs are found at equivalent positions for the human Cep192 sites (*red* boxes), while there is a similar potential motif at an equivalent position to the single *C. elegans* motif (*blue* box). This motif is potentially phosphorylated by Cdk1, so we also mutated a second nearby S-S/T sequence that is conserved in *Drosophila* that could be phosphorylated by Cdk1 (*yellow* box) to generate the Spd-2-AA-mKate2 construct (that we used to test the potential importance of these sites in recruiting Polo to the mitotic PCM).

Figure S6

Distribution of potential Polo binding sites in Spd-2/Cep192 and Cnn/Cep215 protein families. Schematic representation of the amino acid sequences of *D. melanogaster* Spd-2 (1146aa) and *H. sapiens* Cep192 (isoform 1, 1941aa) (*light grey*), and *D. melanogaster* Cnn (1148aa) and *H. sapiens* Cep215/Cdk5Rap2 (1893aa) (*dark grey*).

Because these proteins have different numbers of amino acids, the cartoons have been normalised to the same length for ease of comparison. The position of each S-S/T motif (potential PBD binding site) is indicated with lines underneath each cartoon: *red* lines indicate potential PBD-binding sites that are conserved in at least 11 of 12 *Drosophila* species or 8 of 9 mammalian species; *light blue* lines indicate sites that are less well conserved. Note that the fly and human homologues of Spd-2/Cep192 and Cnn/Cep215 share little sequence identity (~23% and ~24%, respectively), yet the number and overall distribution of potential PBD binding sites is quite similar. Note also that we use Isoform 1 of Cep192 in this comparison, but similar results are obtained with the longer isoform 3 (2537aa), and an analysis of both isoforms is included in the MSAs shown in the accompanying data files.

Figure S7

The models tested in the regression analysis of Spd-2-GFP dynamics during centrosome maturation. The Spd-2-GFP dynamics data for each individual embryo (see Figure 8, and Figures S5 and S6) was assessed using the nonlinear regression (curve fit) analysis function in GraphPad Prism 7. The different functions used are illustrated schematically in the graphs. R^2, adjusted R^2, and absolute sum-of- square values are used as a measure for goodness-of-fit. **(A)** The data for WT Spd-2-GFP was fitted against four different functions to assess the most suitable model: (1) user-defined linear growth followed by linear decrease; (2) user-defined linear growth followed by plateau followed by linear decrease; (3) Gaussian function; (4) Lorentzian function. The preferred model was (2). **(B)** The data for Spd-2-CONS-GFP was fitted against the

preferred model for the WT data (2), but the data seemed to be described better as a straight line, so it was also fitted against two additional models: (5) a standard straight line; (6) a user-defined linear constant line. The preferred model was (5), although the average slope value was nearly zero (-0.0005 $\pm$ 0.0054; mean $\pm$ SD), indicating that the appropriate model in practice would be (6), a constant line.

References

Allan, C., Burel, J.-M., Moore, J., Blackburn, C., Linkert, M., Loynton, S., Macdonald, D., Moore, W.J., Neves, C., Patterson, A., et al. (2012). OMERO: flexible, model-driven data management for experimental biology. Nat Methods *9*, 245–253.

Aydogan, M.G., Wainman, A., Saurya, S., Steinacker, T.L., Caballe, A., Novak, Z.A., Baumbach, J., Muschalik, N., and Raff, J.W. (2018). A homeostatic clock sets daughter centriole size in flies. J Cell Biol *217*, 1233–1248.

Ball, G., Demmerle, J., Kaufmann, R., Davis, I., Dobbie, I.M., and Schermelleh, L. (2015). SIMcheck: a Toolbox for Successful Super-resolution Structured Illumination Microscopy. Sci Rep *5*, 15915.

Basto, R., Brunk, K., Vinadogrova, T., Peel, N., Franz, A., Khodjakov, A., and Raff, J.W. (2008). Centrosome amplification can initiate tumorigenesis in flies. Cell *133*, 1032–1042.

Bodenmiller, B., Malmstrom, J., Gerrits, B., Campbell, D., Lam, H., Schmidt, A., Rinner, O., Mueller, L.N., Shannon, P.T., Pedrioli, P.G., et al. (2007). PhosphoPep—a phosphoproteome resource for systems biology research in Drosophila Kc167 cells. Mol Syst Biol *3*.

Buszczak, M., Paterno, S., Lighthouse, D., Bachman, J., Planck, J., Owen, S., Skora, A.D., Nystul, T.G., Ohlstein, B., Allen, A., et al. (2006). The Carnegie Protein Trap Library: A Versatile Tool for Drosophila Developmental Studies. Genetics *175*, 1505–1531.

Callan, M.A., Cabernard, C., Heck, J., Luois, S., Doe, C.Q., and Zarnescu, D.C. (2010). Fragile X protein controls neural stem cell proliferation in the Drosophila brain. Human Molecular Genetics *19*, 3068–3079.

Conduit, P.T., and Raff, J.W. (2010). Cnn dynamics drive centrosome size asymmetry to ensure daughter centriole retention in Drosophila neuroblasts. *20*, 2187–2192.

Conduit, P.T., Feng, Z., Richens, J.H., Baumbach, J., Wainman, A., Bakshi, S.D., Dobbelaere, J., Johnson, S., Lea, S.M., and Raff, J.W. (2014a). The centrosome-specific phosphorylation of Cnn by Polo/Plk1 drives Cnn scaffold assembly and centrosome maturation. Dev Cell *28*, 659–669.

Conduit, P.T., Richens, J.H., Wainman, A., Holder, J., Vicente, C.C., Pratt, M.B., Dix, C.I., Novak, Z.A., Dobbie, I.M., Schermelleh, L., et al. (2014b). A molecular mechanism of mitotic centrosome assembly in Drosophila. Elife *3*, e03399.

Dix, C.I., and Raff, J.W. (2007). Drosophila Spd-2 recruits PCM to the sperm centriole, but is dispensable for centriole duplication. *17*, 1759–1764.

Feng, Z., Caballe, A., Wainman, A., Johnson, S., Haensele, A.F.M., Cottee, M.A., Conduit, P.T., Lea, S.M., and Raff, J.W. (2017). Structural Basis for Mitotic Centrosome Assembly in Flies. Cell *169*, 1078–1089.e13.

Giansanti, M.G., Bucciarelli, E., Bonaccorsi, S., and Gatti, M. (2008). Drosophila SPD-2 is an essential centriole component required for PCM recruitment and astral-microtubule nucleation. *18*, 303–309.

Habermann, K., Mirgorodskaya, E., Gobom, J., Lehmann, V., Müller, H., Blümlein, K., Deery, M.J., Czogiel, I., Erdmann, C., Ralser, M., et al. (2012). Functional Analysis of Centrosomal Kinase Substrates in Drosophila melanogaster Reveals a New Function of the Nuclear Envelope Component Otefin in Cell Cycle ….

Koenig, T., Menze, B.H., Kirchner, M., Monigatti, F., Parker, K.C., Patterson, T., Steen, J.J., Hamprecht, F.A., and Steen, H. (2008). Robust prediction of the MASCOT score for an improved quality assessment in mass spectrometric proteomics. J. Proteome Res. *7*, 3708–3717.

Lehmann, V., Müller, H., and Lange, B.M.H. (2006). Immunoisolation of centrosomes from Drosophila melanogaster. Curr Protoc Cell Biol *Chapter 3*, Unit3.17.

Lucas, E.P., and Raff, J.W. (2007). Maintaining the proper connection between the centrioles and the pericentriolar matrix requires Drosophila centrosomin. J Cell Biol *178*, 725–732.

Matsuda, A., Schermelleh, L., Hirano, Y., Haraguchi, T., and Hiraoka, Y. (2018). Accurate and fiducial-marker-free correction for three-dimensional chromatic shift in biological fluorescence microscopy. Sci Rep *8*, 7583.

Novak, Z.A., Conduit, P.T., Wainman, A., and Raff, J.W. (2014). Asterless licenses daughter centrioles to duplicate for the first time in Drosophila embryos. Curr. Biol. *24*, 1276–1282.

Novak, Z.A., Wainman, A., Gartenmann, L., and Raff, J.W. (2016). Cdk1 Phosphorylates Drosophila Sas-4 to Recruit Polo to Daughter Centrioles and Convert Them to Centrosomes. Dev Cell *37*, 545–557.

Raff, J.W., Kellum, R., and Alberts, B. (1994). The Drosophila GAGA transcription factor is associated with specific regions of heterochromatin throughout the cell cycle. Embo J *13*, 5977–5983.

Roberts, E.B. (1998). Drosophila A Practical Approach (Oxford University Press).

Tinevez, J.-Y., Perry, N., Schindelin, J., Hoopes, G.M., Reynolds, G.D., Laplantine, E., Bednarek, S.Y., Shorte, S.L., and Eliceiri, K.W. (2016). TrackMate: An open and extensible platform for single-particle tracking. Methods *115*, 80–90.

Waterhouse, A.M., Procter, J.B., Martin, D.M.A., Clamp, M., and Barton, G.J. (2009). Jalview Version 2--a multiple sequence alignment editor and analysis workbench. Bioinformatics *25*, 1189–1191.

Zhai, B., Villén, J., Beausoleil, S.A., Mintseris, J., and Gygi, S.P. (2008). Phosphoproteome analysis of Drosophila melanogaster embryos. J. Proteome Res. *7*, 1675–1682.

Figure S1

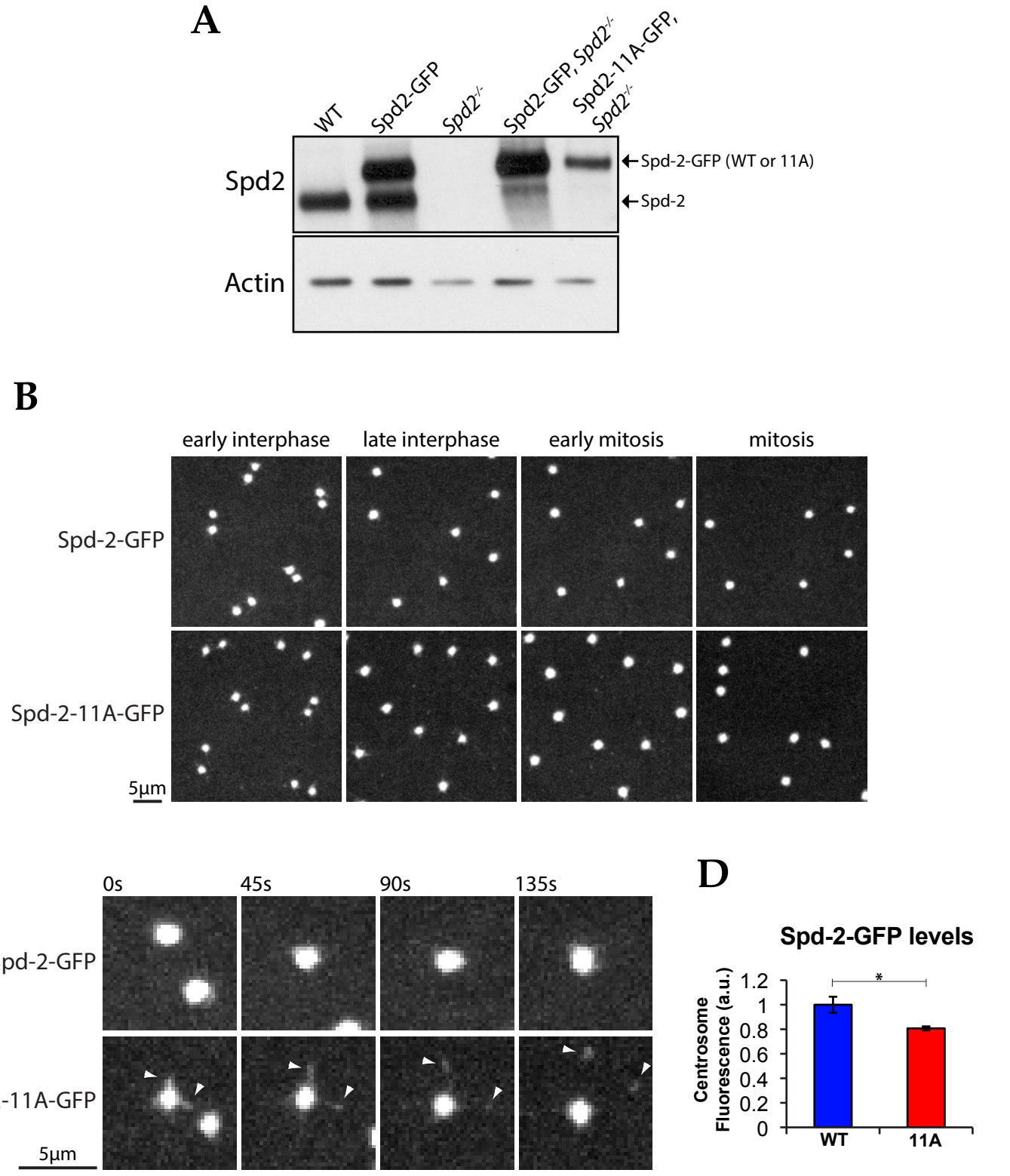
A
WT
Spd2-GFP
Spd2-/-
Spd2-GFP, Spd2-/-
Spd2-11A-GFP, Spd2-/-
Spd2
Actin
Spd-2-GFP (WT or 11A)
Spd-2
B
early interphase
late interphase
early mitosis
mitosis
Spd-2-GFP
Spd-2-11A-GFP
5µm
C
0s
45s
90s
135s
Spd-2-GFP
Spd-2-11A-GFP
5µm
D
Spd-2-GFP levels
Centrosome Fluorescence (a.u.)
1.2
1
0.8
0.6
0.4
0.2
0
*
WT
11A

Figure S2

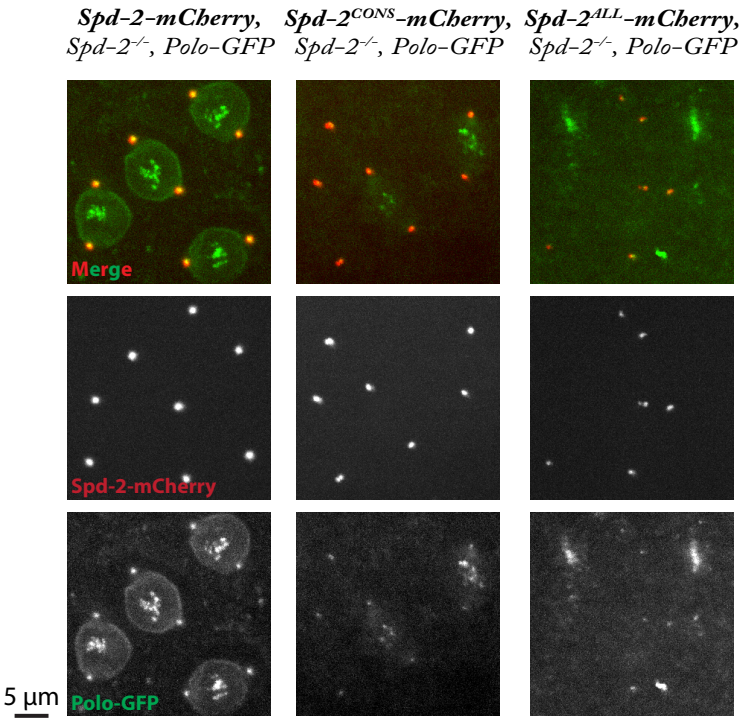
Spd-2-mCherry, Spd-2-/-, Polo-GFP
Spd-2CONS-mCherry, Spd-2-/-, Polo-GFP
Spd-2ALL-mCherry, Spd-2-/-, Polo-GFP
Merge
Spd-2-mCherry
Polo-GFP
5 µm

Figure S3

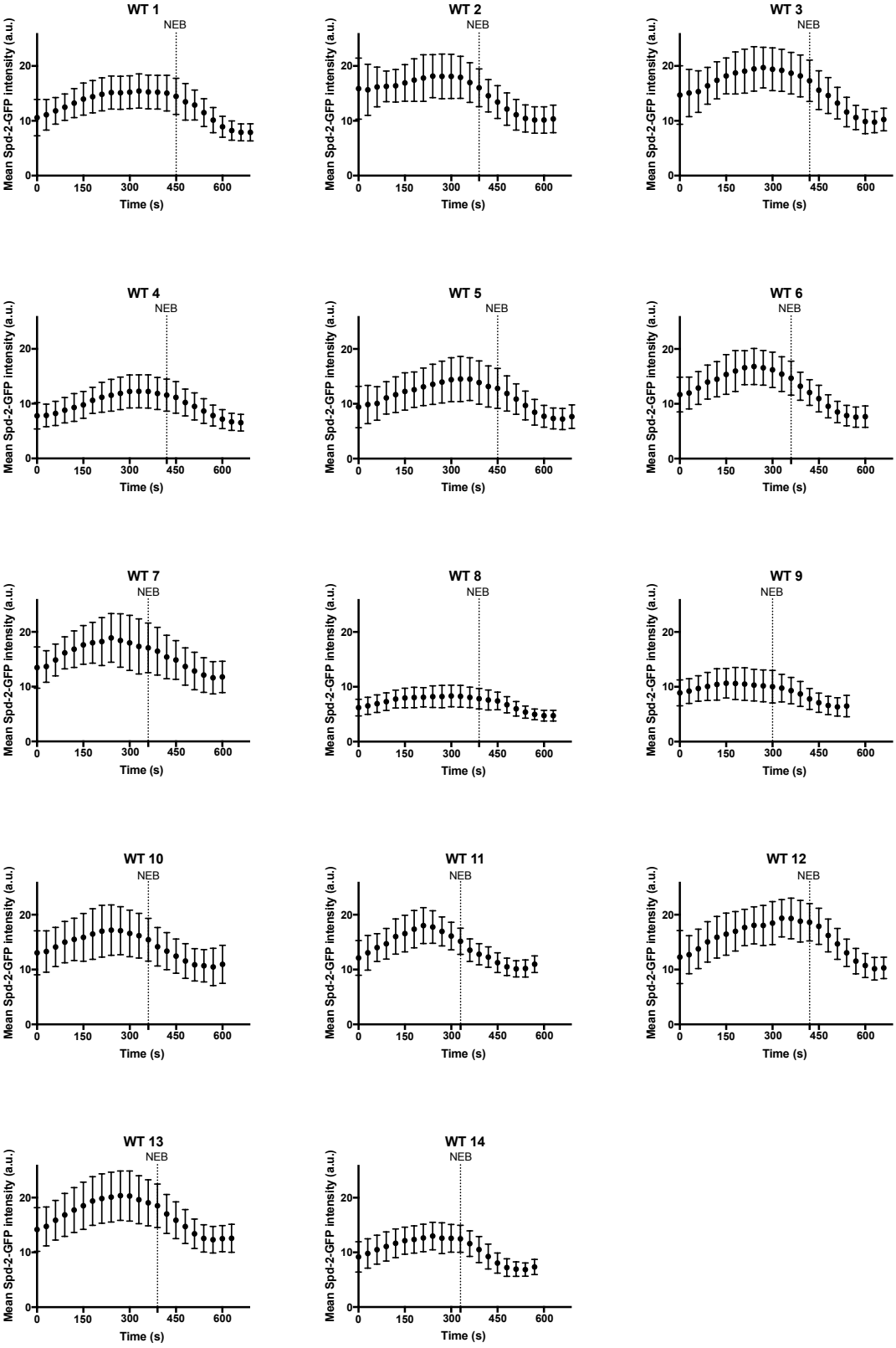
WT 1
WT 2
WT 3
WT 4
WT 5
WT 6
WT 7
WT 8
WT 9
WT 10
WT 11
WT 12
WT 13
WT 14
NEB
Mean Spd-2-GFP intensity (a.u.)
Time (s)
0
10
20
0
150
300
450
600

Figure S4

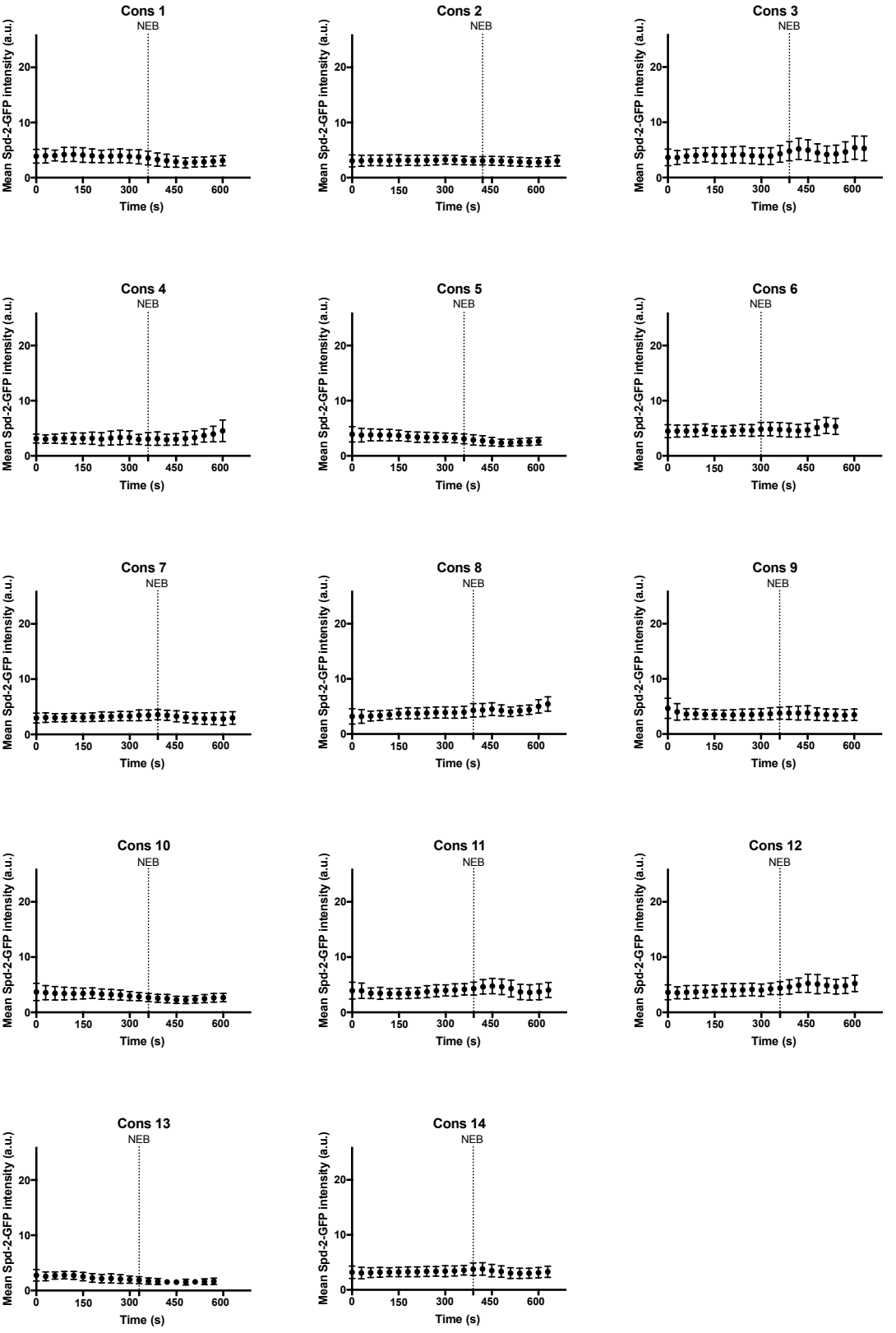
Cons 1
Cons 2
Cons 3
Cons 4
Cons 5
Cons 6
Cons 7
Cons 8
Cons 9
Cons 10
Cons 11
Cons 12
Cons 13
Cons 14
NEB
Mean Spd-2-GFP intensity (a.u.)
Time (s)
0
10
20
150
300
450
600

Figure S5

Figure S6

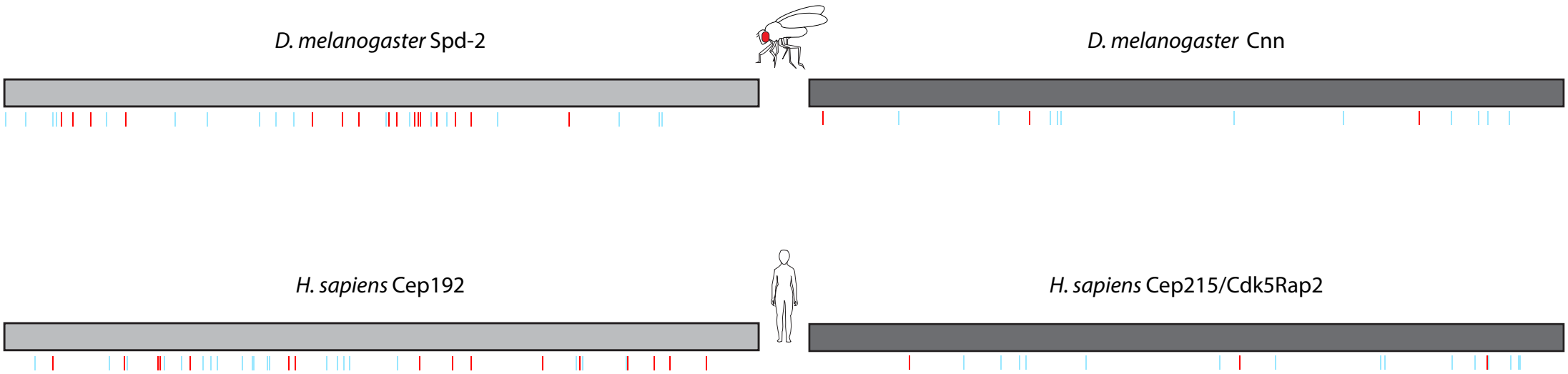

| = Potential PBD-binding site that is well conserved in other species

| = Potential PBD-binding site that is not well conserved in other species

Figure S7

A

Spd-2-WT-GFP data set N = 14 embryos	Increase - Decrease (1) 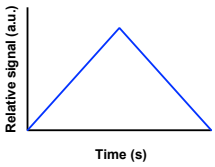	Increase - Plateau - Decrease (2) 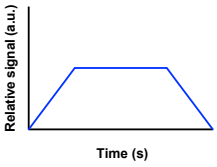	Gaussian (3) 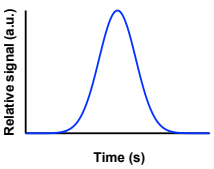	Lorentzian (4) 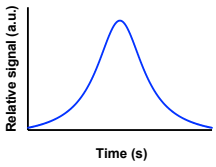
R^2 value	0.96 ± 0.03	0.99 ± 0.01	0.96 ± 0.02	0.96 ± 0.02
R^2 value (adjusted)	0.96 ± 0.03	0.98 ± 0.02	0.96 ± 0.02	0.96 ± 0.03
$SS_{Absolute}$	2.23 ± 1.62	0.87 ± 0.61	2.91 ± 2.40	3.16 ± 2.92
% of fit preference	14.3%	64.3%	7.1%	14.3%

B

Spd-2-CONS-GFP data set N = 14 embryos*	Increase - Plateau - Decrease (2) 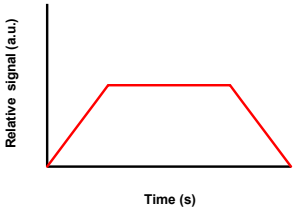	Straight line (5) 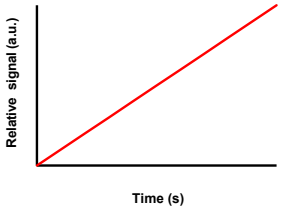	Constant (6) 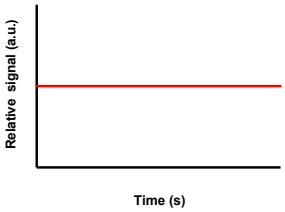
R^2 value	0.70 ± 0.29	0.51 ± 0.37	N/A
R^2 value (adjusted)	0.62 ± 0.38	0.48 ± 0.39	N/A
$SS_{Absolute}$	0.50 ± 0.60	0.69 ± 0.58	2.43 ± 1.71
% of fit preference	14.3%	57.1%	28.6%

*Data from 2 embryos did not converge for Increase – Plateau – Decrease model